

Journal of Materials Chemistry C

Accepted Manuscript



This is an *Accepted Manuscript*, which has been through the Royal Society of Chemistry peer review process and has been accepted for publication.

Accepted Manuscripts are published online shortly after acceptance, before technical editing, formatting and proof reading. Using this free service, authors can make their results available to the community, in citable form, before we publish the edited article. We will replace this *Accepted Manuscript* with the edited and formatted *Advance Article* as soon as it is available.

You can find more information about *Accepted Manuscripts* in the [Information for Authors](#).

Please note that technical editing may introduce minor changes to the text and/or graphics, which may alter content. The journal's standard [Terms & Conditions](#) and the [Ethical guidelines](#) still apply. In no event shall the Royal Society of Chemistry be held responsible for any errors or omissions in this *Accepted Manuscript* or any consequences arising from the use of any information it contains.



Temperature-dependent shape-responsive fluorescent nanospheres for image-guided drug delivery

Shawn He,¹ George Tourkakis,¹ Oleg Berezin,² Nikolay Gerasimchuk,³ Hairong Zhang,¹ Haying Zhou,¹ Asaf Izraely,⁴ Walter J. Akers,¹ Mikhail Y. Berezin^{1,5}

Received 00th January 20xx,
Accepted 00th January 20xx

DOI: 10.1039/x0xx00000x

www.rsc.org/

Temperature-responsive nanoparticles used in conjunction with hyperthermia promise to provide synergistic effects for increasing drug efficacy. We propose a near-infrared (NIR) fluorescent system based on an upper critical solution temperature (UCST) polymer, ISP2, integrated with a NIR fluorescent dye HITC for in vivo tracking. The system forms a nanoparticle that increases its volume as temperature increases, similar to the expansion of a Hoberman sphere. The nanospheres nearly doubled in size, from 80 nm to 140 nm, during a temperature increase from 40 °C to 60 °C

1. Introduction

Local and systemic thermal therapies are promising tools for the treatment of life-threatening diseases such as cancer. These techniques encompass a variety of strategies, from whole-body hyperthermia treatments to spatially controlled localized heating. The range of heating varies from slightly above the physiologic body temperature in hyperthermia treatments, where even mild temperature increases can lead to tumour cell apoptosis and stimulation of the immune system,¹ to high-temperature thermal ablations that cause the instantaneous death of tumour cells.²⁻⁴

One strategy for thermal treatments is based on combining these techniques with chemotherapy.⁵ Elevated temperatures render blood vessels and the cell membranes more susceptible to penetration by chemotherapy drugs, and therefore more vulnerable to treatments. As a result, mild heating is often used in conjunction with chemotherapy delivery in fever-range whole-body hyperthermia,⁶ regional perfusion,⁷ and hyperthermic intraperitoneal chemotherapy (HIPEC).⁸ This approach might be especially attractive to the use of nanoparticles as drug delivery vehicles, as higher temperatures increase the tissue extravasation from a maximum of 100 nm at 34 °C to >400 nm at 42 °C.⁹

The synergistic effect of hyperthermia with chemotherapy might be further enhanced by using drugs that are activated by temperature. The activation mechanism could include the

change from the inactive prodrug to the pharmacologically active form through thermally induced enzymatic mechanisms,¹⁰ or through a temperature-controlled release of the cargo from nanoformulations. The latter category includes liposomes composed from lipids with physiologically relevant gel-to-liquid phase transition temperatures,^{11, 12} temperature-sensitive dendrimers,¹³ micro- and nanogels made from lower critical solution temperature (LCST)¹⁴ polymers such as PNIPAM¹⁵ or upper critical solution temperature (UCST) polymers.

We envisioned that efficient release of the cargo under thermal conditions might be enhanced through temperature-sensitive nanoparticles that experience substantial shape changes. In this design, nanoparticles with an encapsulated cargo undergo a size increase similar to a Hoberman sphere. A relatively small change in the diameter of the sphere leads to large pore openings, allowing the cargo either to interact with the environment or to leak out. Although polymers that undergo temperature-induced shape changes are known (i.e. the FDA approved polymer Pluronic F-127¹⁶), many of them form nanoparticles that shrink upon heating, which might have limited applications in vivo.¹⁷

As the first step toward the design and testing of the temperature-responsive nanoparticles, we developed a fluorescent nanosphere that could be tracked in vivo. The nanospheres described in this work were spontaneously formed from mixing a temperature responsive polymer ISP2 (**Fig. 1**) with a near-infrared (NIR) dye HITC (**Fig. 2**). Strong and predictable environmental sensitivity of the dye reflected the changes induced by the polymer, enabling the study of the nanospheres in vitro and in vivo. These new nanoparticles showed a desirable size increase, from ca. 80 nm to more than 140 nm during a temperature increase from 40 °C to 60 °C.

¹Department of Radiology, Washington University School of Medicine, St. Louis, MO, USA

²Mobicem Scientific Engineering, LTD, Israel

³Chemistry Department, Missouri State University, Springfield, MO, USA

⁴Albaad Massuot Yitzhak Ltd, Israel

⁵Institute of Materials Science & Engineering, Washington University, St. Louis, MO, USA

*Contact author: berezinm@wustl.edu

2. Experimental details

2.1 Materials

ISP2 (in ethanol/water or water) was prepared according to ref¹⁸ (see synthesis). Solvents: DMSO, ethanol, and high purity water were used throughout the work. Dyes ICG (Indocyanine green, Cardiogreen (Sigma-Aldrich)), HITC iodide and DOTC iodide (both from Exciton), were used without purification. Monomers, initiator and polyacrylic acid sodium salt (MW=8,000) were received from Sigma-Aldrich. Fetal Bovine Serum was obtained from ThermoFisher Scientific.

2.2 Synthesis of ISP2

ISP2 was prepared by radical polymerization of four monomers in ethanol/water solvent system in a glass round-bottom flask reactor (5 L) equipped with a thermometer, a nitrogen insert, a condenser and an overhead stirrer with a Teflon propeller. The reactor was placed into the water bath with heater and a temperature controller. In a typical procedure, acrylic acid (55 g), butyl acrylate (30 g), 2-ethyl hexyl acrylate (15 g) and diethyleneglycol monoallyl ether (12 g) were dissolved in a solvent mixture formed by 108 g of ethanol and 38 g water under the constant flow of nitrogen. The mixture was heated to 65 °C under stirring. An initiator 2,2'-azobis (2-amidinopropane) dihydrochloride (0.88 g in 5 g of water) was added into the reactive mixture at once. During the exothermic part of reaction, the temperature increased up to 85-82 °C for 15 min, resulting in the ~75% conversion. Complete conversion was reached after 2 hours of heating at 70 °C. The reactor was cooled to 40 °C, and solution of 4 g of NaOH in 400 mL water was added for partial neutralization of the carboxylic groups of the formed polymer. The polymer solution in water: ethanol (80:20 w/w) appeared milky at room temperature and transparent above 40 °C. The mixture was further evaporated under vacuum to remove most of ethanol. The residual level of ethanol in the final composition was less than 2%, as measured by GC. Final composition (20% of the polymer in water) was viscous and transparent at all temperatures. Molecular weight of the polymer was MW=10,000 Da as measured with gel permeation chromatography (GPC), polydispersity index PDI=4-6. The polymer is currently available from Mobichem Engineering Ltd (Israel).

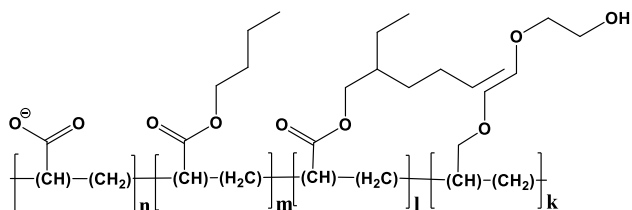


Fig. 1. Structure of the polymer ISP2 comprised from four monomers (randomly connected): acrylic acid, butyl acrylate, 2-ethylhexyl acrylate and diethyleneglycol monoallyl ether (0.95:0.3:0.1:0.1, mol fraction). MW=10,000 Da measured with GPC, PDI= 4-6.

2.3 Synthesis of ISP2 based nanoparticles

ISP2 was dissolved in water to form concentrations of 10 mg/mL as stock solution. An aliquot of ISP2/water stock solution (20 μ L) was further mixed with 400 μ L water or saline solutions in a 1.5

mL Eppendorf tube, followed by vortexing for 30 sec. The solutions were stored at -20°C. Stock solutions of HITC, ICG or DOTC (1 mg/mL) were prepared in DMSO. Fluorescent nanoparticles dye-ISP2 were synthesized by mixing 1 mL of ISP2 stock solution with the appropriate amount of the dye stock solution, followed by vortexing for 30 sec. In the case of HITC, the nanoparticles were prepared in the range of concentrations from 1 nmol HITC/mg ISP2 to 25 nmol HITC/mg ISP2 (from 10 to 250 nmol HITC/mol of ISP2). Nanoparticles were stored at -20°C.

2.4 Dynamic light scattering (DLS)

Hydrodynamic diameter measurements were performed on a Malvern Nano-ZS Zetasizer (Malvern Instruments Ltd.). The 4 mW helium-neon laser was operated at 633 nm with the scatter angle fixed at 173°. After the formation of dye-ISP2 nanoparticles (30 sec), samples of 100 μ L solutions were immediately loaded into a Malvern DTS1060C cuvette without dilution. Samples were vortexed for 5 sec between each measurement. The measurements were conducted with an equilibration time of 120 sec at the preset temperatures (25 to 65 °C), with 3 measurements for each sample. Each data point contained an average of 16 scans.

2.5 Scanning electron microscopy (SEM)

For SEM analysis, a drop of sample was placed on the FEI Nova Nano 230 SEM pin stub specimen mount covered with double coated carbon conductive tabs and dried under high vacuum at ca. 10 min. The studied samples were coated with a 5 nm gold-layer using a Cressington 108 Gold Sputter Coater.

2.6 Absorption and fluorescence measurements

Absorption spectra were measured using spectrophotometer DU-640 (Beckman-Coulter). Fluorescence measurements were performed using Nanolog (Horiba). Samples of 1 mL solution were loaded into 1.5 mL polystyrene disposable cuvettes. Emission spectra were captured using an excitation wavelength of 670 nm, emission range of 685-900 nm. Absolute quantum yield was measured in quartz cuvettes in a Quanta- ϕ 6" integrating sphere coupled with the Nanolog spectrophotometer via a fibre bundle (Horiba). Fluorescence anisotropy was measured in quartz cuvettes using a K2 spectrophotometer (ISS Inc.) equipped with a temperature-controlled cuvette holder (Northwest Quantum) with excitation at 670 nm and emission at 760 nm, conducted in L-format with automated Glan-Thompson polarizing prisms and averaged from 10 trials performed for each measurement.

2.7 Fluorescence lifetime measurements

Fluorescence lifetime measurements were determined using the time-correlated single photon counting (TCSPC) as we previously described.¹⁹ A steady state 740 nm NanoLED was used for excitation, with emission measured at 790 nm. Samples of nanospheres were diluted with water to absorbance 0.3 au measured by the spectrophotometer DU-640 (Beckman-Coulter). Instrument response functions were recorded using solutions of Ludox HS-40 (Sigma-Aldrich) added to water to match the sample's alpha-value, with emission wavelength set

to 740 nm. Analysis of fluorescence lifetime was performed using a two-exponential fitting algorithm implemented in DAS6 software (Horiba).

2.8 Fluorescent orientation polarizability Δf

The function Δf was derived from a combination of dielectric constants (ϵ) and refractive indexes (n) according to eq.1.

$$\Delta f = \frac{\epsilon - 1}{2\epsilon + 1} - \frac{n^2 - 1}{2n^2 + 1} \quad \text{eq. 1}$$

2.9 Flow cytometry

Flow cytometry measurements were performed using a FACScan flow cytometer (Beckman Coulter) equipped with 10 fluorescent channels including a 637 nm argon ion laser and a 660/20-nm bandpass filter. Laser power was set to 1060 mW; PMT Gain for fluorescence detection was 353; Side scattering PMT Gain was 388. The results were processed with FlowJo X software package.

2.10 Gel-permeation chromatography (GPC)

Molecular mass of the polymer was measured using GPC (ThermoFisher Scientific), eluent DMF /0.01 M LiCl, column – GRAM (PSS Polymer Standards Service GmbH), temperature of measurement 70 °C.

2.11 Differential scanning calorimetry/Thermal analysis (DSC/TG)

Thermal properties of ISP2 were measured using Q-600 analyser (TA Instruments) in the range of 20 – 1600 °C under high purity N₂ gas with flow rate 100 mL/min. The sample mass was 12.15 mg. The rate of sample heating was 2 degrees/minute. Data processing was carried out using TA Universal Analysis software package.

2.12 In vivo Imaging

All animal studies were conducted according to protocols approved by the Washington University Animal Studies Committee. Female FVB mice were anesthetized with isoflurane (2% in O₂) and carefully shaved and depilated to remove hair overlying dorsum. In vivo optical imaging was performed with the Pearl NIR imaging system (LICOR Biosciences) and ex vivo imaging performed with Multispectral FX Pro preclinical imaging system (Bruker). Fluorescence ($\lambda_{\text{ex/em}} = 780/810$ nm) and brightfield images were acquired immediately after injection of either HITC or HITC-ISP2 and sequentially up to 60 min post-injection. After imaging, animals were humanely euthanized by cervical dislocation while fully anesthetized. Organs were dissected and placed on a clear plastic petri dish for imaging. Brightfield and NIR fluorescence ($\lambda_{\text{ex/em}} = 760/830$ nm) images were acquired and overlaid to demonstrate differential accumulation of fluorescent compounds.

3. Results and Discussion

3.1 HITC dye shows strong environmental sensitivity

HITC (1,3,3,1',3',3'-hexamethyl-2,2'-indotricarbocyanin) is a polymethine Cy7 type dye soluble in a variety of media and often studied as a model fluorescent compound,²⁰⁻²³ laser

dye,²³ precursor to optical materials²⁴ and a contrast agent in biological applications.²⁵ As a typical cyanine dye, HITC showed absorption-fluorescence sensitivity to the environment, including spectral shifts (Fig. 2), change in fluorescence anisotropy, and change in fluorescence lifetime (Table 1). In a surrounding media with lower solvent orientation polarizability function (Δf), HITC as other cyanine dyes exhibit absorption and emission bathochromic shifts as well as longer fluorescence lifetimes (solvatochromism).²⁶⁻²⁸ Similar behaviour (bathochromic shift, longer fluorescence lifetime) was also observed for HITC-ISP2 nanoparticles.

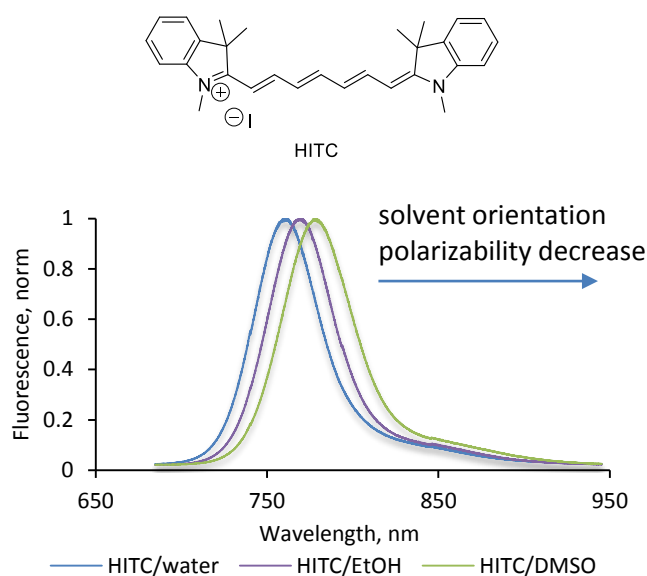


Fig. 2 Structure of HITC and its emission spectra in solvents of different polarity (solvent orientation polarizability). The arrow shows the direction of the shift with the increase of solvent orientation polarizability

Table 1 Fluorescent properties of HITC in different environments

Media	Δf	μ , cP	$\lambda_{\text{max}}^{\text{abs}}$	$\lambda_{\text{max}}^{\text{em}}$	r	τ , ns	Φ , %
water	0.320	0.894	736	760	0.14	0.40	5.1
ethanol	0.289	1.074	743	772	0.08	1.01	15.8
DMSO	0.263	1.996	750	777	0.12	1.31	20.8
ISP2*			750	775	0.32	1.12	12.9

Δf - solvent orientation polarizability, $\lambda_{\text{max}}^{\text{abs}}$ - absorption maxima, $\lambda_{\text{max}}^{\text{em}}$ - emission maxima, r - fluorescence anisotropy, τ - fluorescence lifetime, ns; Φ - absolute quantum yield, *) in water

We have previously established a correlation between Δf and optical properties of Cy7 type dyes (spectral shifts, fluorescence lifetime) and applied this correlation for determining micropolarities within micelles, nanoparticles and protein binding sites.²⁹⁻³⁴ In the case of HITC, the emission shift was small but noticeable (17 nm) from 760 nm in water to 777 nm in less polar DMSO (and in the presence of ISP2), while the change in the fluorescence lifetime was quite significant, increasing from 0.4 ns in water to 1.3 ns in DMSO and 1.12 ns in ISP2. While the absolute change of a dipole moment value is a major reason for the observed spectral shifts, conformational

stability of the excited molecule was the most critical factor affecting fluorescence lifetime.^{33, 35}

The role of viscosity was marginal, as judged by fluorescence anisotropy values that did not correlate with the solvent viscosity (Table 1). This correlates with our previous results demonstrating that cyanine dyes are rather poor rotors.³⁶

In principle, fluorescence shifts of HITC observed in the presence of ISP2 might be also caused by oppositely charged acrylic residues in the polymer. The commercial form of HITC has an iodide as a counterion. Replacement of iodide can potentially lead to the shift in the emission. However, we observed no spectral displacement after the addition of an excess of NaCl or polyacrylic acid (PAA). The latter has similar to ISP2 molecular weight (MW=8,000) and charge. Thus, the observed shifts and the changes of other optical parameters of HITC in the presence of the ISP2 polymer were attributed to the change in the microenvironment's polarity-type properties around the fluorophore due to encapsulation.

3.2 ISP2 is a temperature sensitive polymer

ISP2 polymer is comprised from four monomers: acrylic acid, butyl acrylate, 2-ethyl hexyl acrylate and diethyleneglycol monoallylether, polymerized by radical polymerization in water – ethanol solution.¹⁸ The polymer is formed through mixing the monomers prior to polymerization, leading to a randomized composition. Despite its random non-crosslinked structure, the polymer undergoes a relatively sharp, physiologically relevant phase transition at 43.5 °C (Fig. 3), which makes it attractive for temperature-sensitive applications.

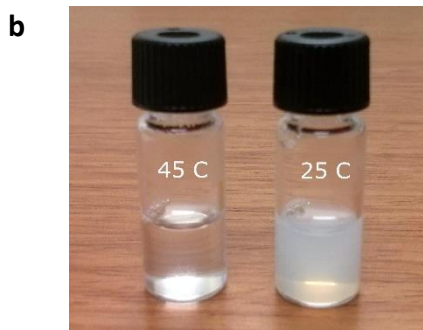
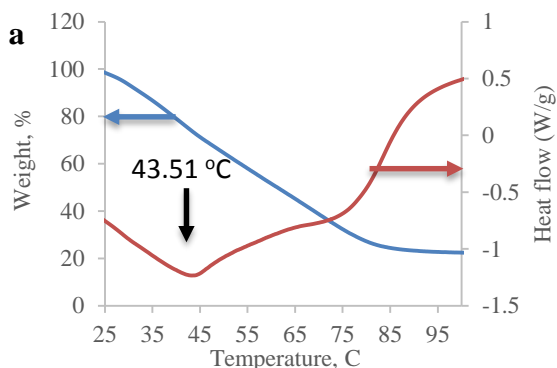


Fig. 3 Temperature sensitive polymer ISP2 (16% polymer concentration in water/ethanol 80:20 w/w). a: DSC/TG measurements for ISP2 showing phase transition temperature at 43.5 °C: red – sample's weight loss; blue – heat flow. There is a continuous weight loss to ~90 °C due to sample dehydration that is not coupled with the phase transition. b: Change in polymer transparency from 25°C to 45°C due to the conformational change.

The observed thermo-sensitivity of the polymer nanoparticles reflects a known but rare class of water-soluble UCST polymers.³⁷⁻³⁹ This class of temperature-sensitive macromolecules undergoes a coil–globule transition below the critical temperature, leading to a change in conformation from an expanded coil state (open configuration, transparent solution) to a collapsed globule state (close configuration, cloudy solution). The negative peak at 43.5°C indicates a conversion of a two-phase globular system (non-solvated state) into a monophasic coil-type structure of the polymer (solvated state). At the lowest point of this endothermic peak, the system is in equilibrium, and hence the change in the Gibbs free energy is close to zero ($\Delta G = \Delta H - T\Delta S \approx 0$, $\rightarrow \Delta H \approx T\Delta S$). The sign of the peak suggests an endothermic process with $\Delta H > 0$ pointing to a positive change in entropy $\Delta S > 0$, which is expected for the globule–to–coil transition characteristic for UCST polymers.⁴⁰

3.3 ISP2 forms nanoparticles in response to ions

The ISP2 polymer exhibited ion-sensitive shape changes in ionic solutions. In pure water, the size of the nanoparticles was quite small, ca. 5 nm, and increased to 10 nm in 0.9% NaCl solution. The size of the nanoparticle was further increased in higher saline concentration, to ca. 70 nm at 4.5% NaCl (Fig. 4). The solutions of the nanoparticles were found to be quite stable, as longitudinal measurements by DLS did not reveal significant alterations in the particle size distribution after a week of storage.

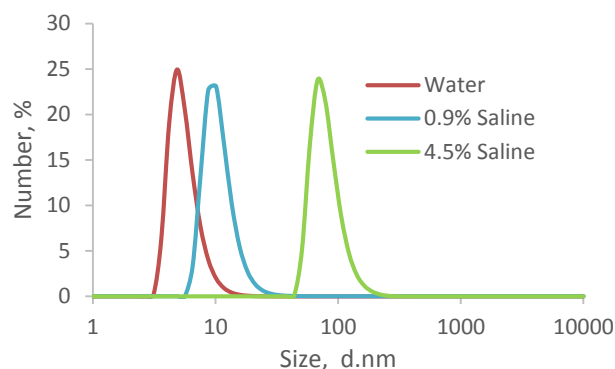


Fig. 4 DLS measurements of ISP2 in water and saline at r.t. show nanoparticle formation with size dependent on saline concentration

The results of the flow cytometry experiments are shown in Fig. 5 and corroborate the DLS study. The presence of saline at 0.9% caused small changes in both FSC (front scattering) and SSC (side scattering) channels, apparently because of the relatively small changes in the nanoparticle size (from 5 to 10 nm). In contrast, a higher level of saline concentration (4.5%) caused a significant shift in the FSC signal accompanied by an increase of more than an order of magnitude in front scattering intensity. SSC showed an even more dramatic change of almost four orders of magnitude higher in concentrated saline than in water, suggesting the formation of uniform nanoparticles.

We suggested that the observed shape-responsive behaviour was due to the decrease in the number of hydrogen bonds between the solvent water molecules (salting out effect). This effect results from the formation of ion–water hydration

complexes, which in turn decreases hydration and the solubility of the polymer.⁴¹ Therefore, the nanoparticles feature a hydrophobic core made from butyl acrylate and 2-ethyl hexyl acrylate, and a hydrophilic shell composed from acrylic acid and diethylene glycol ether. Given the shape responsive properties of the polymer in the presence of ions, we hypothesized that the nanoparticles can be also formed in the presence of charged dye molecules with an appropriate hydrophobicity.

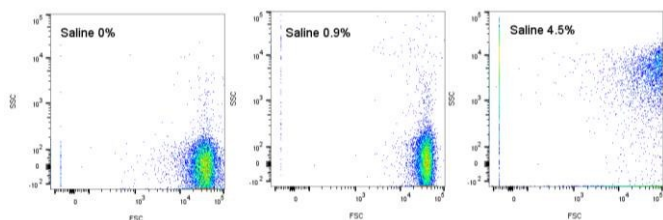


Fig. 5 Flow cytometry of ISP2 in water and saline demonstrates formation of nanoparticles at high saline concentration.

3.4 HITC induces nanosphere formation with ISP2: SEM study

Addition of HITC to an ISP2 polymer solution in water caused an almost instantaneous formation of spherical nanoparticles, as shown in SEM images (**Fig. 6**, b-c). The size of the particles in SEM were consistent with the values obtained using DLS (40-90 nm) and largely independent from the dye-to-polymer ratio in the range from 1 to 25 nmol of HITC /mg of polymer (**Fig. 6**, d).

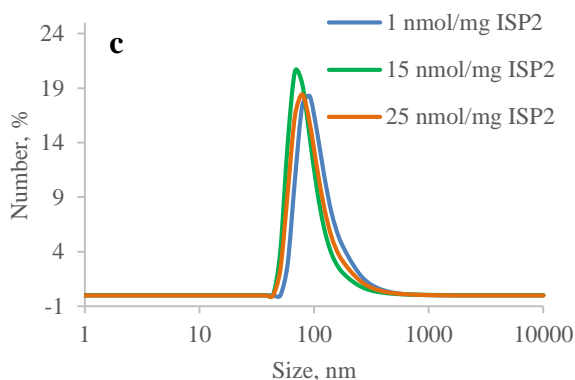
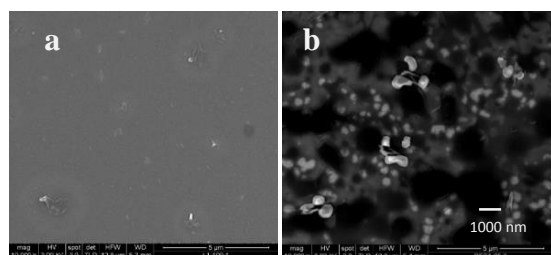


Fig. 6 Particle size of the HITC-ISP2 construct. a) SEM images of ISP2 with no dye, b) SEM images of ISP2 with HITC (10 nmol HITC/mg ISP2), c) DLS of HITC-ISP2 nanospheres in water as function of dye:polymer ratio. Polymer concentration was kept the same for all measurements (10 mg/mL)

In contrast, ICG, a common FDA approved near-infrared dye, did not form stable nanoparticles above 10 nm (**Fig. S2**, Supplementary Information) apparently due to an overall negative charge of the ICG molecule (see the structure in **Fig.**

S2.) The corresponding autocorrelation curves were of poor quality, indicating a low level of nanoparticle formation. DOTC (**Fig. S2**) has a similar to HITC structure and predictably formed nanoparticles with similar size of ca. 50 nm diameter.

Formation of nanoparticles around HITC was confirmed by steady state and dynamic fluorescence spectroscopy. Mixing of HITC with the polymer led to a ca. 15 nm bathochromic shift of HITC absorption/emission maxima accompanied by a substantial increase in quantum yield and brightness (**Fig. 7**, **Table 1**). These shifts along with the longer fluorescence lifetime from 0.4 ns to 1.12 ns suggested a change in the environment around the fluorophore from an aqueous to a hydrophobic one.^{33, 42} An increased level of fluorescence anisotropy (FA) from 0.14 for the free dye to 0.32 in the presence of the polymer confirmed the tight association of the dye and the polymer, as the larger size resulted in decreased tumbling of the fluorophore. All these experiments unequivocally pointed to the encapsulation of the dye inside the polymer. The relatively large size of the nanoparticle (>50 nm) suggested that several polymer molecules were wrapped around the fluorophores.

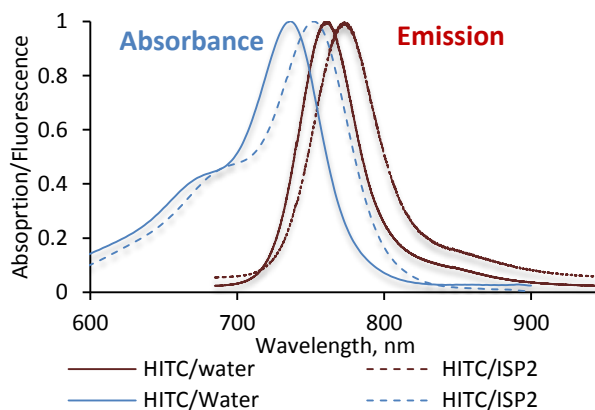


Fig. 7 Fluorescent properties of HITC (10 nmol) with and without the presence of ISP2 in water. Addition of the polymer to HITC (10 nmol HITC/1 mg ISP2) solution causes ca. 15 nm bathochromic shift and 2.5-fold increase of HITC brightness.

The flow cytometry results from HITC-ISP2 nanospheres were similar to those seen in the saline (**Fig. 8**, a-b). Overall change in FSC was rather marginal, while the SSC signal increased dramatically. In addition, fluorescence emission of the nanoparticles increased, reflecting the encapsulation of the fluorescent dye. The sample with the polymer alone, either in water or in the presence of saline, did not show any fluorescence in the NIR channel (**Fig. 8**, c). In contrast, HITC-ISP2 constructs revealed strong emission at a wavelength longer than 740 nm corresponding to the emission of HITC (**Fig. 8**, d). This emission was not uniform, with two dominant populations, and apparently reflected heterogeneity in the nanosphere composition (often referred as granularity).

The size of the HITC-ISP2 nanoparticles also depends on the ionic strength of the solution. As shown in **Fig. S3**, Supplementary Information, with the concentration of NaCl increase, HITC-ISP2 nanoparticles experienced an increase in their size, up to 50% in their diameters. Most of the changes

occurred below 0.75% NaCl. At all studied saline concentrations, (up to 0.9%, corresponding to a physiological solution that essentially isotonic with tissue fluids or blood) nanoparticles remained stable with no apparent collapse. The absence of a hypsochromic shift in HITC-ISP2 emission confirms nanoparticles stability even at relatively high salt concentration (Fig. S4).

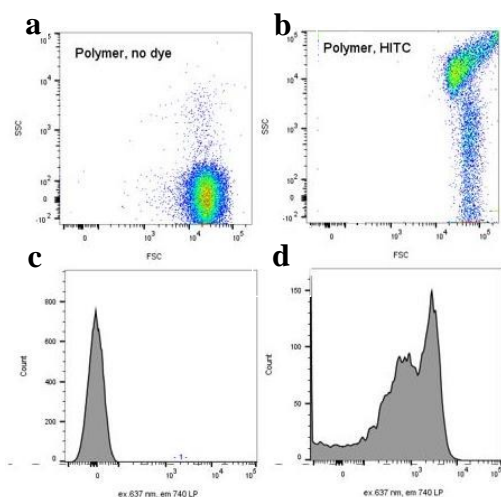


Fig. 8 Flow cytometry of HITC-ISP2 (concentration 10 nmol HITC/1mg of ISP2)

3.5 HITC-ISP2 are shape-responsive temperature sensitive nanospheres

Having established the formation of the nanoparticles around the fluorophore, we tested how the size of the nanospheres changed as a function of temperature. The phase transition of the polymer occurs at 43.5 °C as indicated by a pronounced endothermic peak (Fig. 3). We inferred that this change in temperature would lead to the larger size of the resulting nanoparticles. As expected, DLS measurements (Fig. 9, a-b) demonstrated the substantial increase in the particles' diameter from ~80 nm at 40 °C to 140 nm at 65 °C.

3.6 HITC-ISP2 is stable in vitro and in vivo

The goal of the first step toward temperature-responsive drug delivery system was to prepare temperature-sensitive nanospheres with a NIR fluorescent reporter for tracking the nanospheres in vivo. One of the tasks was to ensure that the change in temperature does not lead to the release of the dye from the polymeric matrix. FA can distinguish between the free dye and dye that is encapsulated into nanoparticles. If release occurs, then the FA value (r) of the released dye would become equal to the r of the free dye. As shown in Fig. 10, this convergence did not occur.

The r -value of the nanoparticle did not become lower, and even slightly increased (reflecting the change in the particle size), suggesting that no release occurred. These results advocate for the high affinity of the dye to the polymer due to hydrophobic-hydrophobic interactions, additionally enhanced through the charge-complex formation between the positively charged dye and the negatively charged PAA residues in the ISP2 polymer.

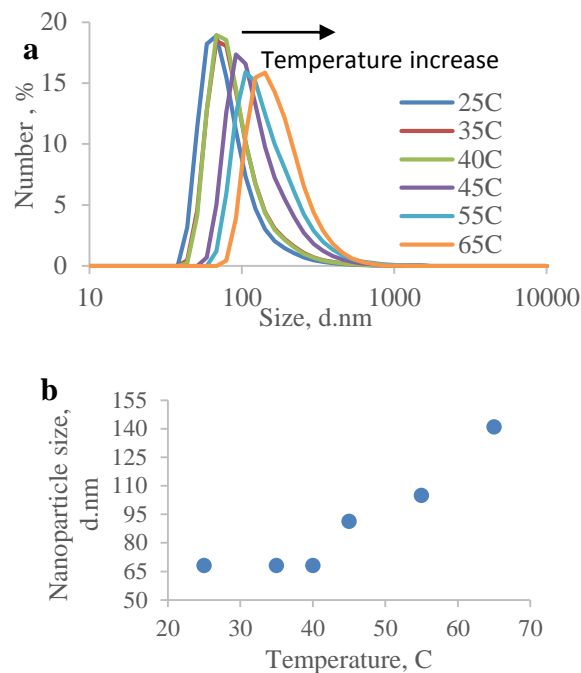


Fig. 9 Thermally induced change of HITC-ISP2. a) The change in nanoparticle size as a function of temperature as measured by DLS. b) The change in the nanoparticle size occurs at the phase transition between 40 and 45 °C

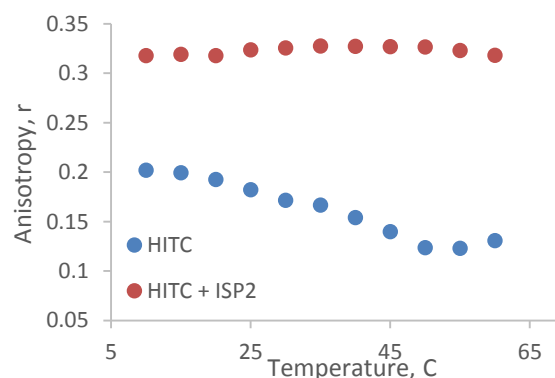


Fig. 10 Fluorescence anisotropy (FA) of HITC and HITC-ISP2 as a function of temperature. The data shows no release of the dye from the nanoparticle at high temperatures. Concentration 10 nmol HITC/mg ISP2 in water. Ex 670 nm, em. 760 nm.

As we have previously observed, these interactions can be disrupted due to the presence of serum proteins.³² Our spectroscopy study showed that it is not the case. An addition of serum to a free HITC dye leads to a substantial bathochromic shift (10 nm) (Fig. S5, Supplementary Information) and an increase in the fluorescence anisotropy values from 0.140 to 0.212 indicating opsonisation of the dye by serum proteins (Table S1, Supplementary Information). In contrary, addition of serum to HITC-ISP2 complexes caused a negligible shift in the emission. The fluorescence anisotropy values were, however, substantially higher (0.287) than in the case of HITC in serum (0.212) reflecting the stability of the HITC-ISP2 complexes in the presence of serum and indicating that the dye is still within the polymer. Slightly reduced anisotropy value of HITC-ISP2 in the

presence of serum (from 0.32 to 0.287) however, might indicate some leakage of the dye, although this change might be instrumental due to the change in optical properties of the solution with relatively high concentration of serum proteins.

To test the stability of the HITC-ISP2 *in vivo*, we injected the construct into a mouse and compared against the distribution of free HITC. After a few minutes, both HITC and HITC-ISP2 spread over the whole body of the animal (**Fig. 11, a-b**). That indicates that the nanoconstruct can effectively deliver the potential cargo to every part of the body. After 1 hour, most of the signals from both HITC and the nanospheres were localized (**Fig. 11, c-d**).

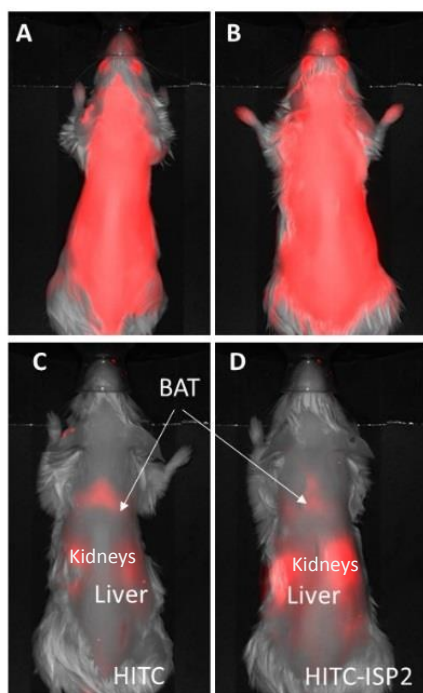


Fig. 11 *In vivo* testing of HITC-ISP2 in mice demonstrates the initial spread of the fluorescence across the whole body. NIR fluorescence images (ex 780/em 810 nm) immediately and 60 min after intravenous injection of (a) HITC post injection (PI) 3 min, (b) HITC/ISP2 PI 3 min, (c) HITC- PI 60 min, (d) HITC-ISP2 PI 60 min. (Same dosage and concentration 10 nmol HITC/mg ISP2)

In vivo studies supported the *in vitro* observations, showing different biodistribution patterns between the free dye and the nanoparticle. The results of the biodistribution 1 hour post-injection shown in **Fig. S6**, Supplementary Information, revealed: i) higher level of HITC-ISP2 in blood compared to the free HITC, suggesting lower rate of extravasation of the nanoparticle due to its size; ii) lower level of nanoparticles in the hydrophobic organs such as BAT and the liver, and iii) higher level in the kidney for the HITC-ISP2 due to complex higher hydrophilicity. These observations point to a stability (at least partial) of the nanoparticles under physiological conditions at normal body temperature and supported tight association of the dye with the polymer.

4. Conclusions and Future outlook

Adding the near-infrared reporter HITC to the polymer solution of IST2 in water caused the formation of NIR fluorescent nanospheres with an encapsulated dye in the hydrophobic core, as shown both by fluorescence and size-measuring studies. The mechanism of the encapsulation lies in the combination of the hydrophilic (carboxylic, diethylene glycol), anionic (carboxylic) and hydrophobic (butyl, 2-ethyl hexyl) groups of the polymer. These groups form a "hydrophobic/hydrophilic balance" and a negatively charged environment enabling encapsulation of the positively charged dyes.

The temperature sensitivity of the nanoparticles caused significant size increases at physiologically relevant temperatures similar to the expansion of a Hoberman sphere (although not crosslinked as the Hoberman sphere would suggest). The *in vitro* and *in vivo* studies have demonstrated the stability of the fluorescent nanosphere with minimum release of the fluorescent label into the environment.

Overall, HITC-ISP2 nanoparticles show promise as an imaging drug delivery system that can be thermally activated for the release in areas of induced hyperthermia. The progress in this area will be important in increasing the efficacy of the existing chemotherapy agents, minimizing acute toxicities caused by cancer therapy and eliminating adverse effects that persist after completion of therapy for which no effective treatments exist.

The next step would be to append the construct with another fluorophore with low affinity to the polymer to mimic cargo. The modified nanoconstruct will be tested in animal models combined with localized hyperthermia treatment. Once the release of the cargo at elevated and physiologically relevant temperatures is confirmed, the HITC-ISP2 nanospheres with loaded drugs will be investigated in cancer animal models. We expect that the nanospheres loaded with the anticancer drugs will demonstrate increased effectiveness in image-guided drug delivery during thermally based treatments.

Acknowledgements

We thank the Alvin J. Siteman Cancer Center at Washington University School of Medicine and Barnes-Jewish Hospital in St. Louis, Mo., for the use of the Siteman Flow Cytometry Core, The Siteman Cancer Center is supported in part by an NCI Cancer Center Support Grant #P30 CA91842. We thank the financial support from Missouri EPSCoR Program under NSF Foundation's Research Infrastructure Improvement Award # IIA-1355406. This work was performed in part at the Nano Research Facility (NRF), a member of the National Nanotechnology Infrastructure Network (NNIN), which is supported by the National Science Foundation under Grant No. ECS-0335765. NRF is part of the School of Engineering and Applied Science at Washington University in St. Louis. We also thank the Washington University Optical Spectroscopy Core facility (NIH 1S10RR031621-01) for spectroscopy measurements.

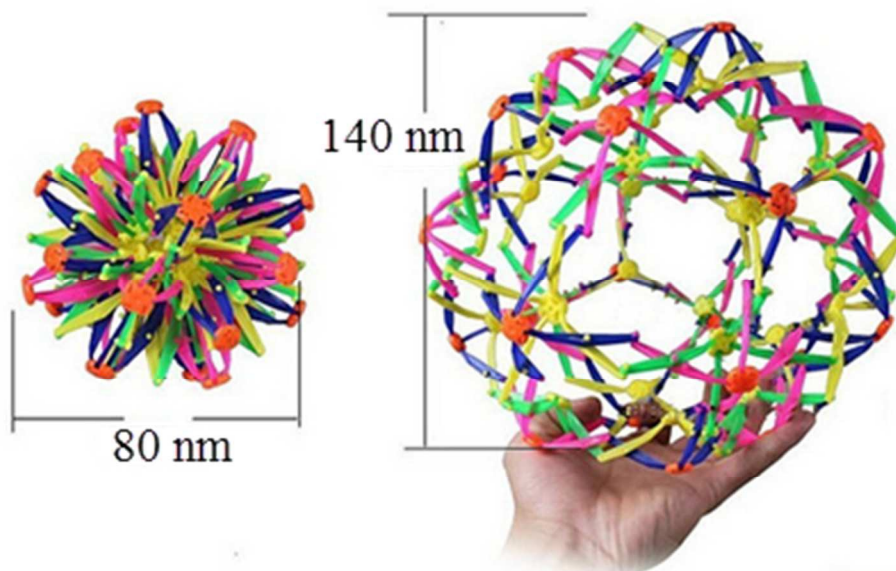
References

1. Y. Kobayashi, Y. Ito, V. V. Ostapenko, M. Sakai, N. Matsushita, K. Imai, K. Shimizu, A. Aruga and K. Tanigawa, *Immunol Lett*, 2014, **162**, 256-261.
2. M. Hurwitz and P. Stauffer, *Semin Oncol*, 2014, **41**, 714-729.
3. J. van der Zee, *Ann. Oncol.*, 2002, **13**, 1173-1184.
4. K. F. Chu and D. E. Dupuy, *Nat Rev Cancer*, 2014, **14**, 199-208.
5. M. Urano, M. Kuroda and Y. Nishimura, *Int J Hyperthermia*, 1999, **15**, 79-107.
6. Y. Xu, J. Choi, B. Hylander, A. Sen, S. S. Evans, W. G. Kraybill and E. A. Repasky, *Int J Hyperthermia*, 2007, **23**, 513-527.
7. L. Qiu, D. K. Pleskow, R. Chuttani, E. Vitkin, J. Leyden, N. Ozden, S. Itani, L. Guo, A. Sacks, J. D. Goldsmith, M. D. Modell, E. B. Hanlon, I. Itzkan and L. T. Perelman, *Nat Med*, 2010, **16**, 603-606, 601p following 606.
8. S. Gonzalez-Moreno, L. A. Gonzalez-Bayon and G. Ortega-Perez, *World J Gastrointest Oncol*, 2010, **2**, 68-75.
9. G. Kong, R. D. Braun and M. W. Dewhirst, *Cancer Res*, 2000, **60**, 4440-4445.
10. K. V. Nemani, R. C. Ennis, K. E. Griswold and B. Gimi, *J Biotechnol*, 2015, **203**, 32-40.
11. L. Zhu, Z. Huo, L. Wang, X. Tong, Y. Xiao and K. Ni, *Int J Pharm*, 2009, **370**, 136-143.
12. K. Kono, K. Yoshino and T. Takagishi, *J Control Release*, 2002, **80**, 321-332.
13. G. Sun and Z. Guan, *Macromolecules*, 2010, **43**, 9668-9673.
14. L. Zhu and V. P. Torchilin, *Integr Biol (Camb)*, 2013, **5**, 96-107.
15. L. Zha, B. Banik and F. Alexis, *Soft Matter*, 2011, **7**, 5908-5916.
16. P. Chandaroy, A. Sen and S. W. Hui, *J Control Release*, 2001, **76**, 27-37.
17. S. H. Choi, S. H. Lee and T. G. Park, *Biomacromolecules*, 2006, **7**, 1864-1870.
18. 2015.
19. N. G. Zhegalova, S. He, H. Zhou, D. M. Kim and M. Y. Berezin, *Contrast Media Mol Imaging*, 2014, **9**, 355-362.
20. M. P. Samtsov, S. A. Tikhomirov, O. V. Buganov, K. N. Kaplevsky, D. G. Melnikov and L. S. Lyashenko, *J Appl Spectrosc*, 2009, **76**, 783-790.
21. M. Y. Berezin, K. Guo, B. Teng, W. B. Edwards, C. J. Anderson, O. Vasalatiy, A. Gandjbakhche, G. L. Griffiths and S. Achilefu, *J Am Chem Soc*, 2009, **131**, 9198-9200.
22. M. P. Samtsov, S. A. Tikhomirov, L. S. Lyashenko, D. S. Tarasau, O. V. Buganov, V. A. Galievsky, A. S. Stasheuski and E. S. Voropay, *J Appl Spectrosc*, 2013, **80**, 170-175.
23. K. Drexhage, 1977.
24. F. del Monte and D. Levy, *Chem Mater*, 1995, **7**, 292-298.
25. F.-s. Wang and F. Kubota, *Cytometry*, 2002, **50**, 267-274.
26. E. Lippert, *Z. Elektrochem. Angew. Phys. Chem.*, 1957, **61**, 962-975.
27. J. R. Lakowicz, *Principles of fluorescence spectroscopy*, Springer, New York, 3rd edn., 2006.
28. N. Mataga, Y. Kaifu and M. Koizumi, *Bull. Chem. Soc. Japan*, 1956, **29**, 465-470.
29. A. Almutairi, W. J. Akers, M. Y. Berezin, S. Achilefu and J. M. Frechet, *Molecular pharmaceuticals*, 2008, **5**, 1103-1110.
30. M. Y. Berezin, H. Lee, W. Akers, G. Nikiforovich and S. Achilefu, *Photochem Photobiol*, 2007, **83**, 1371-1378.
31. S. A. Dergunov, K. Kesterson, W. Li, Z. Wang and E. Pinkhassik, *Macromolecules*, 2010, **43**, 7785-7792.
32. T. P. Gustafson, S. A. Dergunov, W. J. Akers, Q. Cao, S. Magalotti, S. Achilefu, E. Pinkhassik and M. Y. Berezin, *RSC advances*, 2013, **3**, 5547-5555.
33. M. Y. Berezin, H. Lee, W. Akers and S. Achilefu, *Biophys J*, 2007, **93**, 2892-2899.
34. M. Y. Berezin, H. Lee, W. Akers, G. Nikiforovich and S. Achilefu, *Photochemistry and photobiology*, 2007, **83**, 1371-1378.
35. M. Y. Berezin and S. Achilefu, *Chem Rev*, 2010, **110**, 2641-2684.
36. M. Y. Berezin, H. Lee, W. Akers, G. Nikiforovich and S. Achilefu, 2008.
37. J. Seuring and S. Agarwal, *Macromol Rapid Commun*, 2012, **33**, 1898-1920.
38. J. Seuring and S. Agarwal, *ACS Macro Lett*, 2013, **2**, 597-600.
39. D. Roy, W. L. A. Brooks and B. S. Sumerlin, *Chem Soc Rev*, 2013, **42**, 7214-7243.
40. I. U. S. Lipatov and A. E. Nesterov, *Thermodynamics of polymer blends*, Technomic Pub., Lancaster, PA, 1997.
41. R. Sadeghi and F. Jahani, *J Phys Chem B*, 2012, **116**, 5234-5241.
42. I. Texier, M. Goutayer, A. Da Silva, L. Guyon, N. Djaker, V. Jossierand, E. Neumann, J. Bibette and F. Vinet, *J Biomed Opt*, 2009, **14**, 054005.

Temperature-dependent shape-responsive fluorescent nanospheres for image-guided drug delivery

Shawn He, George Tourkakis, Oleg Berezin, Nikolay Gerasimchuk, Hairong Zhang, Asaf Izraely, Haiying Zhou, Walter J. Akers, Mikhail Y. Berezin

Graphical abstract



Nanospheres work similar to Hoberman spheres that undergo significant temperature-induced shape changes revealing large pores (holes) through which drugs released.